PHYSICAL REVIEW B **81**, 245216 (2010)

Group-V impurities in SnO_2 from first-principles calculations

J. B. Varley,[1] A. Janotti,[2] and C. G. Van de Walle[2]
[1]*Department of Physics, University of California, Santa Barbara, California 93106-9530, USA*
[2]*Materials Department, University of California, Santa Barbara, California 93106-5050, USA*
(Received 19 March 2010; revised manuscript received 2 June 2010; published 30 June 2010)

By means of first-principles calculations we investigate the effects of N, P, As, and Sb impurities on the electrical properties of SnO_2. We find that N prefers to occupy the O site and unexpectedly acts as a very deep acceptor with a level closer to the conduction band than to the valence band. P, As, and Sb prefer the Sn site, where they act as shallow donors. The group-V impurities are therefore not suitable for achieving *p*-type conductivity in SnO_2, but P, As, and Sb may serve as *n*-type dopants. We also investigate the interaction between N and H impurities, finding that the binding energy of the N-H complex is much larger than the binding energies found for complexes involving H and group-IIIA impurities in SnO_2.

DOI: 10.1103/PhysRevB.81.245216 PACS number(s): 61.72.Bb, 71.55.Ht, 78.30.Hv

I. INTRODUCTION

SnO_2 is a wide-band-gap material that can be easily doped *n* type, exhibiting high electrical conductivity and optical transparency in the visible range, as well as high reflectivity in the infrared. These combined properties are exploited in a variety of applications, including low-emissivity energy-conserving windows in ovens, antifogging windows in freezers and airplanes, glass touch-sensitive control panels, transparent top-surface electrodes in solar cells, flat-panel displays, and solid-state-lighting devices.[1–4] Although SnO_2 has long been used as a transparent conductor, the effects of the various background impurities and dopants in SnO_2 are largely unknown. As-grown, nominally undoped SnO_2 thin films and bulk crystals typically exhibit *n*-type conductivity, the cause of which has been widely debated. This unintentional conductivity has been traditionally attributed to the presence of native point defects, such as Sn interstitials or O vacancies.[5,6] However, the identification and characterization of these point defects in SnO_2 has been elusive. Recent calculations indicate that oxygen vacancies are deep donors and tin interstitials are unstable, and thus cannot contribute to the observed *n*-type conductivity; instead, the unintentional *n*-type doping is likely to arise from the presence of impurities that act as shallow donors, hydrogen being a prime example.[7]

Gaining better control over *n*-type conductivity in SnO_2 would enhance its performance in current applications. If, in addition, we learn how to make *p*-type SnO_2, it would open a new avenue in semiconductor devices applications. The potential for achieving ambipolar doping in SnO_2 has been discussed in recent studies of group-IIIA impurities (Al,Ga,In) on the Sn site.[7–9] Another possible route for achieving *p*-type doping would consist of incorporating group-VA impurities on the O site. Such an approach has been fiercely pursued, with controversial results, in the case of ZnO, an analogous wide-band-gap material that also has propensity for *n*-type conductivity.[10,11] One should note, however, that group-V atoms have one less valence electron than O and one more valence electron than Sn, thus are expected to show amphoteric behavior in SnO_2. They may act as acceptors when substituting on the O site, but as donors if incorporated on the Sn site. In fact, Sb has been successfully used to achieve high levels of *n*-type doping in SnO_2.[12,13]

In the present paper we perform first-principles electronic-structure calculations to investigate the effects of N, P, As, and Sb impurities on the electronic properties of SnO_2, focusing on their behavior as acceptors or donors. We find that the group-V impurities will not give rise to *p*-type conductivity: P, As, and Sb preferentially incorporate on the Sn site and act as donors while N on the O site is a very deep acceptor.

II. METHODS

A. Computational details

The electronic-structure calculations were performed using the generalized Kohn-Sham theory with the screened hybrid functional of Heyd, Scuseria, and Ernzerhof (HSE).[14] In this approach, a fraction of Hartree-Fock (HF) exchange potential is mixed with the exchange potential of the generalized-gradient approximation of Perdew, Burke, and Ernzerhof (PBE).[15] The HSE hybrid functional has been shown to produce lattice constants, band gaps, and formation enthalpies in improved agreement with experimental values, as compared to other functionals such as PBE and PBE0.[16] The standard value of the characteristic screening length was used [10 Å (Ref. 14)], and the HF mixing parameter was set to 32% to yield good agreement with the experimental band gap of SnO_2.[17] Use of the correct band gap is important for an accurate description of the electronic-structure and formation energies of defects.[11,18] The "default" mixing parameter of 25% leads to an underestimation of the band gap by 0.6 eV; use of 32% mixing facilitates a direct comparison with experimental values for defect levels in the band gap.[11] We have verified, however, that all of our main conclusions are independent of the mixing parameter. Specifically, the deep or shallow nature of the dopants is not affected by this choice.

The effects of spin polarization were included in all calculations that involved unpaired electrons. The electron-ion interactions were treated using projector augmented wave potentials as implemented in the VASP code.[19–21] In order to

 ©2010 The American Physical Society

reduce the computational cost of the HSE calculations, the Sn 4*d* electrons were treated as core electrons. The validity of this approximation was checked by performing tests explicitly treating the Sn 4*d* electrons as valence states: formation energies and transition levels were found to be changed by less than 0.1 eV.

Impurities were studied using 72-atom supercells, a $2\times2\times2$ grid of Monkhorst-Pack special k points for the integrations over the Brillouin zone,[22] and a plane-wave basis sets with an energy cutoff of 400 eV. Tests with 216-atom supercells showed that atomic relaxations are well described (to within 0.02 eV) with 72-atom supercells. Corrections for the finite-size-cell effects in the calculations of charged impurities were explicitly taken into account by following the procedure described in Ref. 23.

This correction method requires a knowledge of the static dielectric constant ε_0. We use a value $\bar{\varepsilon}=\frac{1}{3}(2\varepsilon^{\perp}+\varepsilon^{\parallel})$ which averages over the directions perpendicular and parallel to the c axis of rutile SnO_2. Calculations of the static dielectric constant ε_0 (including ionic contributions) are currently not included in the VASP code. We calculated the electronic contribution in the random-phase approximation, neglecting the local field effects, obtaining $\varepsilon_\infty^{\perp}=3.07$ and $\varepsilon_\infty^{\parallel}=3.33$. We then estimated theoretical values of ε_0 using the ratio between the experimental values of ε_0 (13.5 and 9.58, Ref. 24) and ε_∞ (3.78 and 4.17, Ref. 24), obtaining a value of $\bar{\varepsilon}_0=9.86$. We have checked that our results are insensitive to the precise value of the dielectric constant: the charge-state corrections change by less than 50 meV when we use the $\bar{\varepsilon}_0^{exp}$ value as opposed to the theoretical value.

B. Formation energies and chemical potentials

Formation energies are key quantities from which we can derive impurity concentrations and solubilities, stability of different charge states of a given impurity and the related electronic transition levels. The equilibrium concentration of an impurity or defect is determined by its formation energy according to $c=N\exp(-\beta E^f)$, where $\beta=k_BT$ and N is the number of available sites for the impurity to incorporate on. The formation energy of an impurity X occupying the O site in SnO_2 is given by

$$E^f[X_{\mathrm{O}}^q]=E_t[X_{\mathrm{O}}^q]-E_t[\mathrm{SnO_2}]+\mu_{\mathrm{O}}-\mu_X+q\epsilon_F, \quad (1)$$

where $E_t[X_{\mathrm{O}}^q]$ is the total energy of the supercell containing the impurity X (X=N, P, As, or Sb) in the charge state q, and $E_t[SnO_2]$ is the total energy of a perfect crystal in the same supercell. For charged impurities, electrons are exchanged with the electron reservoir in the solid, whose energy corresponds to the Fermi level ϵ_F that is conventionally referenced to the valence-band maximum (VBM). An additional correction (ΔV) is included to account for the proper alignment of the reference in the defect supercell, as described in Refs. 23 and 25, resulting in an overall Fermi-level term $\epsilon_F=\epsilon_{\mathrm{VBM}}+\Delta V+\tilde{\epsilon}_F$, where $\tilde{\epsilon}_F$ ranges over the band gap.

The impurity X is taken from a reservoir with energy $\mu_X=E_t[X_{\mathrm{bulk}}]+\tilde{\mu}_X$, and the O atom is placed in a reservoir with energy $\mu_{\mathrm{O}}=\frac{1}{2}E_t[\mathrm{O_2}]+\tilde{\mu}_{\mathrm{O}}$. The chemical potentials ($\tilde{\mu}$) can vary to correspond to the experimental conditions during growth or annealing, which can range from O-rich (Sn-poor) to O-poor (Sn-rich) conditions. We reference their values to the energy per atom of isolated O_2 and N_2 molecules, and to the elemental bulk phases of Sn, P, As, and Sb (white Sn, red P, and black As). Bounds are imposed on the chemical potentials so as to ensure the stability of SnO_2 while avoiding the formation of secondary phases Sn_mX_n, i.e., Sn_3N_4, Sn_3P_4, Sn_3As_4, and Sn_3Sb_4

$$\tilde{\mu}_{\mathrm{Sn}}+2\tilde{\mu}_{\mathrm{O}}=\Delta H_f(\mathrm{SnO_2}), \quad (2)$$

$$m\tilde{\mu}_{\mathrm{Sn}}+n\tilde{\mu}_X<\Delta H_f(\mathrm{Sn}_mX_n). \quad (3)$$

The O-poor limit is characterized by $\tilde{\mu}_{\mathrm{Sn}}=0$, $\tilde{\mu}_{\mathrm{O}}=\frac{1}{2}\Delta H_f(\mathrm{SnO_2})$, and $\tilde{\mu}_X<\frac{1}{n}\Delta H_f(\mathrm{Sn}_mX_n)$. Similarly, the O-rich limit is defined by $\tilde{\mu}_{\mathrm{O}}=0$, $\tilde{\mu}_{\mathrm{Sn}}=\Delta H_f(\mathrm{SnO_2})$, and $\tilde{\mu}_X<\frac{1}{n}[\Delta H_f(\mathrm{Sn}_mX_n)-m\Delta H_f(\mathrm{SnO_2})]$ (or $\tilde{\mu}_X<0$). We also considered SnO as a potential limiting phase but found that it does not affect our results.[7] From the formation enthalpies of the relevant phases Sn_mX_n, the above relations show that the lowest formation energy (i.e., highest solubility) of an impurity X substituting on the O site occurs in the O-poor limit.

An expression similar to Eq. (1) can be written for X substituting on the Sn site. In this case the boundaries on the chemical potentials are given by the formation enthalpy of the X_nO_m phases

$$n\tilde{\mu}_X+m\tilde{\mu}_{\mathrm{O}}<\Delta H_f(X_n\mathrm{O}_m), \quad (4)$$

where the appropriate limiting phases are P_2O_5, As_2O_5, and Sb_2O_5. In this case, O-rich conditions are found to be *less* favorable for incorporation of X on the Sn site provided that $m>2n$, a condition which is satisfied here.

Similar formation-energy expressions can be written for interstitial H and H-acceptor complexes in SnO_2, with the hydrogen reservoir reference taken as molecular hydrogen. In the O-rich limit, the solubilities of H-related species are limited by the formation of H_2O, i.e., $\tilde{\mu}_{\mathrm{O}}+2\tilde{\mu}_{\mathrm{H}}<\Delta H_f(\mathrm{H_2O})$. In the O-poor limit, the solubility of N is limited in the presence of interstitial H by the formation of NH_3, i.e., $\tilde{\mu}_{\mathrm{N}}+3\tilde{\mu}_{\mathrm{H}}<\Delta H_f(\mathrm{NH_3})$, thus resulting in different N-H binding energies under O-rich and O-poor conditions. Because of their positive enthalpy of formation phosphine (PH_3) and arsine (AsH_3) do not impose further restrictions on $\tilde{\mu}_{\mathrm{H}}$.[26]

C. Transition levels

In addition to determining impurity solubilities, the formation energies also provide information on the transition levels between different charge states of the impurities, corresponding to the thermal ionization energies. The transition level between charge states q and q' is defined as

$$\epsilon(q/q')=\frac{E^f[X^q;\tilde{\epsilon}_F=0]-E^f[X^{q'};\tilde{\epsilon}_F=0]}{q'-q}, \quad (5)$$

which are represented by kinks in the plots of formation energy as a function of Fermi level.[25] It is from these transition levels or ionization energies that we can predict whether a given defect will act as a donor or an acceptor for a particular range of Fermi level.

TABLE I. Calculated structural parameters a, c, and u, bulk modulus B_0, band gap E_g, and formation enthalpy ΔH_f of SnO_2.

	Theory	Experiment
E_g (eV)	3.50	3.60[a]
a (Å)	4.74	4.74[b]
c (Å)	3.18	3.19[b]
u	0.306	0.306[b]
B_0 (GPa)	220	218[c]
ΔH_f (eV/f.u.)	−5.74	−6.02 [d]

[a]Reference 17.
[b]Reference 27.
[c]Reference 28.
[d]Reference 29.

III. RESULTS AND DISCUSSION

A. Bulk properties

SnO_2 is most stable in the rutile crystal structure, in which the Sn atom has six nearest-neighbor O atoms, and the O atom has three nearest neighbor Sn atoms. This structure is characterized by two lattice parameters a and c, and an internal parameter u that defines the Sn-O distance in the plane perpendicular to the c direction. The calculated properties of bulk SnO_2 are listed in Table I. The lattice parameters and bulk modulus are in excellent agreement with experiment. The equilibrium c/a and u parameters give rise to 4 Sn-O longer bonds (2.055 Å) and 2 Sn-O shorter bonds (2.051 Å), consistent with analysis from neutron-diffraction measurements.[27]

The calculated direct band gap is 3.50 eV, close to the experimental value of 3.597 eV.[17] Our calculations treat the Sn $4d$ states as core electrons. HSE calculations (32% mixing) in which the Sn $4d$ states are treated as valence states show that the hybrid functional treatment greatly improves the position of the d states: the averaged d band is located 21.7 eV below the VBM for 32% mixing, which compares well with reported experimental values of 21.5 eV (Ref. 30) and 22.5 eV (Ref. 31). A PBE calculation would underestimate the binding energy of the d states and place them at 20.5 eV below the VBM. Even when the d states are treated as core states, the use of projector augmented wave potentials[21] effectively includes their effects on band structure and structural properties. Indeed, a comparison between d-in-the-core and d-in-the-valence HSE calculations shows that structural parameters are changed by less than 0.1% and features in the band structure (such as the band gap) by less than 0.1 eV.

Other properties of the electronic structure, such as the dispersion and valence-band width, are also in good agreement with experimental results and are largely independent of the HF mixing used or the explicit treatment of the Sn $4d$ electrons as valence states. From the conduction-band dispersion along the Γ-Z and Γ-X directions, we obtain electron effective masses of $m_{\parallel}^{*}=0.273m_0$ and $m_{\perp}^{*}=0.320m_0$ respectfully, in excellent agreement with the experimental values of 0.234 and $0.299m_0$ from submillimeter cyclotron

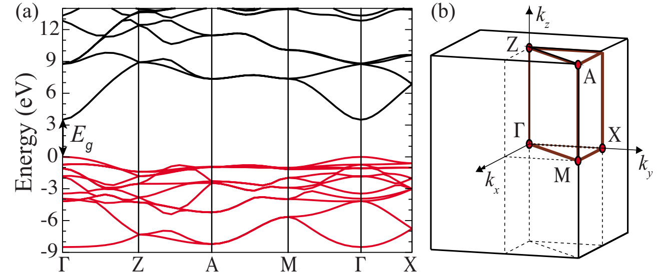

FIG. 1. (Color online) (a) Calculated band structure for SnO_2 using the HSE hybrid functional. The VBM is set to zero on the energy axis. (b) Brillouin zone for rutile, indicating high-symmetry points included in the band-structure plot.

resonance.[32] The hole effective masses were determined to be $1.61m_0$ and $1.37m_0$ for the parallel and perpendicular directions; these values have not yet been determined experimentally. Additionally, as shown in Fig. 1, the calculated valence-band width of 8.5 eV (not including any finite-lifetime or instrumental resolution broadening), is in good agreement with the experimental value of 9 eV from ultraviolet photoemission spectroscopy experiments.[33] We find that both the peak positions and the band width are insensitive to the value of the mixing parameter with the width increasing by only 0.1 eV (toward the experimental value) when the mixing is increased from 25% to 32%.

B. N, P, As, and Sb impurities in SnO_2

In this section we discuss the different impurities individually. Formation energies for all relevant charge states of the substitutional impurities are shown in Figs. 2–6. For each Fermi-level position, only the lowest-energy charge states are shown. As discussed in Sec. II C, the thermal ionization energies or transition levels correspond to the kinks in the formation-energy lines.

1. Nitrogen

Based on atomic size and electronic-structure considerations, N is expected to prefer the O site in SnO_2 and act as

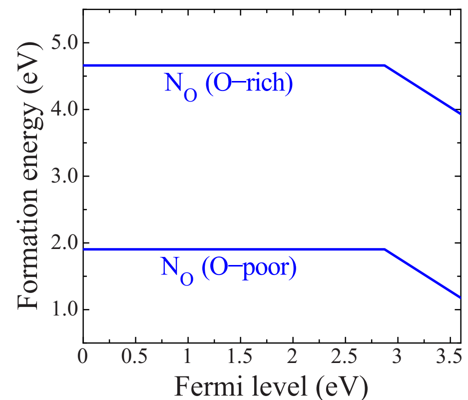

FIG. 2. (Color online) Calculated formation energies for N substituting on the O site in SnO_2 using the HSE hybrid functional. N is found to be highly unstable when substituting on the Sn site. The bounds are shown for the formation energies corresponding to the extremes of O-poor and O-rich limits.

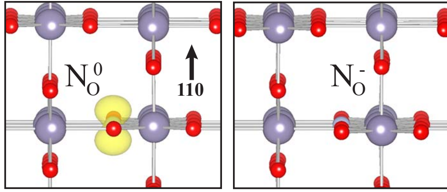

FIG. 3. (Color online) Relaxed configurations of N substituting on the O site in SnO_2 using the HSE hybrid functional. The spin density isosurface, set to 10% of its maximum value, is also shown for the neutral N_O, displaying the highly localized hole state oriented in the 110 direction.

an acceptor. Based on the similarity with oxygen, and since the states at the top of the valence band in SnO_2 are mainly anion derived, we intuitively expect the N-related states to appear near the VBM. However, for N_O in the neutral charge state, we find a singly occupied single-particle state at 1.40 eV above the VBM. Upon including spin polarization, this state splits into an occupied spin-up state at 0.37 eV *below* the VBM, and an unoccupied spin-down state 4.60 eV higher. We attribute this very large spin splitting to the fact that this state is highly localized around the N impurity. Such large spin splittings have been observed in hybrid functional calculations for molecules.[34] This state is derived from the N p orbital oriented perpendicular to the plane containing N and its three nearest-neighbor Sn atoms, as seen in Fig. 3. The states derived from the other two N p orbitals strongly mix with the host states that compose the upper valence band and do not contribute to any other states in the band gap. In the negative charge state, N_O^-, the doubly occupied N-related state lies at 1.54 eV above the VBM.

The calculated formation energies for N_O in SnO_2 are shown in Fig. 2. The transition level $\epsilon(0/-)$ for N_O is located at 2.87 eV above the VBM, meaning that N will be negatively charged only for Fermi-level positions very high in the band gap, near the conduction-band minimum. Therefore, N_O emerges as an extremely deep acceptor. It cannot possibly lead to p-type conductivity in SnO_2. The position of the uppermost N-related state in the band gap is also consistent with the relative energy of the N p and O p atomic orbitals, where the N orbitals are 2.66 eV higher in energy than those of O.[35]

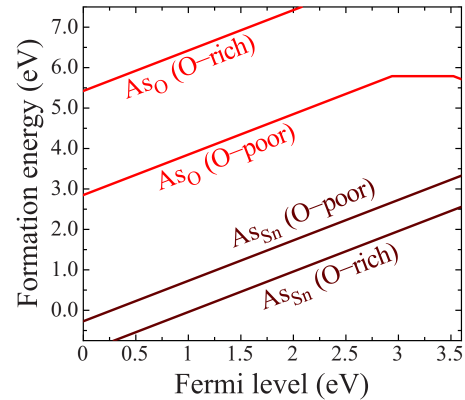

FIG. 5. (Color online) Calculated formation energies for substitutional As-related defects in SnO_2 using the HSE hybrid functional. The bounds are shown for the formation energies corresponding to the extreme O-poor and O-rich limits.

We also analyzed the local lattice relaxations around N_O^0 and N_O^-. In the neutral charge state, the neighboring Sn atoms relax slightly outward, resulting in a Sn-N bond length that is 2% longer than the equilibrium Sn-O bond length. In the N_O^- charge state, the neighboring Sn atoms relax toward the N_O, contracting the bond length by 3% with respect to the equilibrium Sn-O bond length.

Figure 2 shows that the formation energy of the substitutional N_O is lowest in the O-poor limit but still relatively high even in n-type material in which the Fermi level is near the conduction band. This implies a low solubility of N in SnO_2 if N_2 is used as the source of N. We note, however, that higher solubilities could be achieved by using N-plasma or NO gas sources and raising the value of the chemical potential $\tilde{\mu}_N$.

We also explored the possibility of N_O being stable in the positive charge state by removing an electron from the singly occupied state of neutral N_O. We find that N_O^+ is displaced off-site to bond with adjacent O atoms, resulting in a very high formation energy, with a transition level $\epsilon(+/0)$ below the VBM.

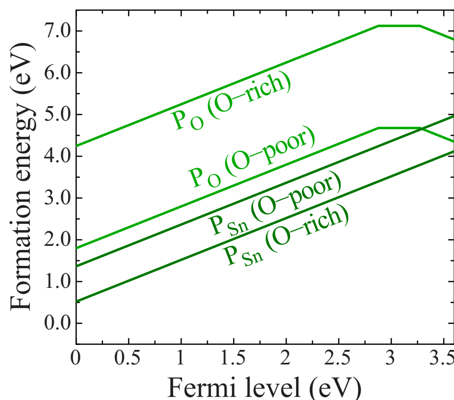

FIG. 4. (Color online) Calculated formation energies for substitutional P-related defects in SnO_2 using the HSE hybrid functional. The bounds are shown for the formation energies corresponding to the extreme O-poor and O-rich limits.

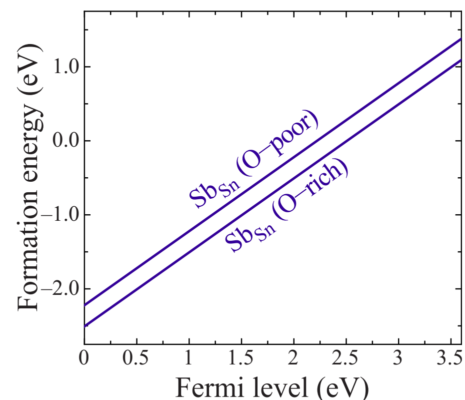

FIG. 6. (Color online) Calculated formation energies for Sb_{Sn} in SnO_2. The Sb_{Sn} defect was found to be considerably higher in formation energy and therefore highly unlikely to form. Both O-rich and O-poor limiting conditions are shown.

Due to the size and electronic-structure mismatch between N and Sn, we expect that N would not occupy the Sn site in SnO_2. Indeed, we find that N_{Sn} is unstable and that the N atom is significantly displaced off site. The relaxed configuration for N_{Sn} can be regarded as a V_{Sn}-N_i complex, with the interstitial N_i bonded to a neighboring O atom. These complexes are very high in energy and are not expected to form in N-doped SnO_2.

To further characterize the N_O defect, we have calculated configuration coordinate diagrams to determine the absorption and emission lines that would result from photoexcitation. We find that optical absorption corresponding to the transition $N_O^- \rightarrow N_O^0$, in which the electron from N_O^- is promoted to the conduction band, occurs with an energy of 1.50 eV. The calculated emission line corresponding to a conduction-band electron recombining with the hole on the neutral N_O^0 is only 0.01 eV, which would be difficult to detect experimentally.[36] Starting from a neutral charge state for nitrogen, we find that to excite electrons from the bulk valence band to the unoccupied level (turning N into N_O^-) would require energies higher than the band-gap energy. For luminescence experiments, we find that an emission line at 2.10 eV would be associated with the transition $N_O^- \rightarrow N_O^0$ with the electron recombining with a hole in the valence band.

2. Phosphorous

Phosphorous is a much larger atom than N, thus making its incorporation on O site in SnO_2 less likely. On the other hand, P is also significantly smaller than Sn and may lead to large lattice relaxations if incorporated on the Sn site. In Fig. 4 we show the calculated formation energies of P_{Sn} and P_O configurations in SnO_2. We find that P_{Sn} is energetically more favorable under most circumstances with P_O being favored over only a narrow range of Fermi levels under O-poor conditions. We also find that P_{Sn} acts as a shallow donor in SnO_2. We find no deep states in the gap and, in the neutral charge state, the extra electron from P_{Sn}^0 occupies a conduction-band-like state, i.e., an extended state that is only slightly perturbed by the presence of the impurity. Therefore, we conclude that P_{Sn} is a shallow donor.

The formation energy of P_{Sn} in *n*-type SnO_2 is quite high even under extreme O-rich conditions. The solubility of P_{Sn} in SnO_2 is limited by the formation of P_2O_5 and the size mismatch between P and Sn. The equilibrium P-Sn bond lengths for P_{Sn}^+ are shorter by 14% with respect to the equilibrium Sn-O bond lengths, yielding P-O bond lengths similar to those found in various phosphorous oxides.[37,38]

For P substituting on the O site in SnO_2, we find that three *p*-derived states appear in the band gap, consistent with the fact that the P *p* orbitals are much higher in energy than the O *p* orbitals.[35] However, the interaction of these orbitals with the surrounding atoms is more complicated than in the case of N_O due to the presence of large lattice relaxations. In the neutral charge state, the highest of these three states is singly occupied and can accept one electron to form P_O^-. We also find that the removal of an electron from the neutral system is possible, with the consequent stabilization of a donor charge state P_O^+, i.e., P_O acts as an acceptor in *n*-type material but as a donor in *p*-type material, in each case counteracting the prevailing conductivity type.

The $\epsilon(+/0)$ and $\epsilon(0/-)$ transition levels associated with P_O are located at 2.88 eV and 3.27 eV above the VBM, respectively, indicating that only in *n*-type conditions is the acceptor state is stabilized. This renders the donor state P_O^+ energetically favorable for Fermi levels over the majority of the band gap.

We find that P_O is significantly displaced off-site, consistent with the large size mismatch between these impurities and O. The planar bonding arrangement to the three nearest-neighbor Sn atoms is unstable, resulting in a lower-symmetry bonding environment with the local distortions highly sensitive to the defect's charge state.

3. Arsenic

Given that arsenic is larger than P, it is expected that As will exhibit an even greater preference for the Sn site than P. The formation energies for As_{Sn} and As_O are shown in Fig. 5. We note, that unlike P, As_{Sn} has lower formation energy than As_O for both O-rich and O-poor conditions. Our calculations indicate that As_{Sn} is a shallow donor, with the extra electron of As_{Sn}^0 occupying a conduction-band-like state. In the case of As_{Sn}^+, the As-O bond lengths are 9% shorter than the equilibrium Sn-O bond lengths, consistent with As being larger than P but still considerably smaller than Sn. As also evident in Figs. 4 and 5, As_{Sn}^+ has significantly lower formation energies than P_{Sn}^+ in SnO_2, indicating a much higher solubility.

For As on the O site, the situation is very similar to that of P, both in terms of the electronic-structure and lattice relaxations, with only minor quantitative differences such as bond lengths and transition-level values. As_O is also significantly displaced off-site with the local relaxations of neighboring O atoms highly sensitive to the charge state of the As_O.

The $\epsilon(+/0)$ and $\epsilon(0/-)$ transition levels for As_O are located at 2.94 eV and 3.52 eV above the VBM, respectively. From these values it is apparent that the acceptor configuration As_O^- is stable only in *n*-type SnO_2. The fact that the $\epsilon(+/0)$ and $\epsilon(0/-)$ levels for As_O are higher in the band gap than those of P_O is consistent with As having *p* orbitals higher in energy than P. Similar to N and P, As is also not suitable for *p*-type doping in SnO_2. We do find, however, that As will substitute on the Sn site with an appreciable solubility and act as a shallow donor.

4. Antimony

Antimony sits to the right of Sn in the periodic table, having an atomic size very close to that of Sn. Thus we expect Sb to preferentially occupy the Sn site in SnO_2, leading to relatively small lattice relaxations, and act as a shallow donor. The calculated formation energies for Sb_{Sn} are shown in Fig. 6. As expected, Sb_{Sn} is shallow donor, stable in the Sb_{Sn}^+ configuration. The extra electron from Sb_{Sn}^0 occupies a conduction-band-like state, perturbed by the presence of Sb. We also find that for Sb_{Sn}^+, the Sb-O bonds are only 3% shorter than the equilibrium Sn-O bond length. The local lattice perturbation associated with Sb_{Sn} is much smaller than those associated with As_{Sn} and P_{Sn}.

As seen in Fig. 6, the formation energy of Sb_{Sn} is lowest under O-rich conditions, where it is limited by the formation of other oxide phases of general stoichiometry Sb_mO_n. As a result, the formation energies of Sb_{Sn} in O-rich and O-poor are very close, due to the stability of the Sb_mO_n phases, which we took as Sb_2O_5 as stated in Sec. II B. Overall, the formation energies for Sb_{Sn}^+ are quite low on an absolute energy scale, implying relatively high solubilities. Sb_{Sn}^+ has notably lower formation energy than As_{Sn}^+ and P_{Sn}^+, thus indicating much higher solubility than As or P in SnO_2. Our results are consistent with experiments in which Sb has been used as an n-type dopant with a 100% ionization efficiency, consistent with a high-solubility shallow donor behavior.[13]

We also explored the possibility of Sb occupying the O site. We find that Sb_O has a very high formation energy even under the most favorable O-poor conditions. As in the case of As_O and P_O, Sb_O is significantly displaced off-site. The lattice distortions associated with Sb_O are even larger than for P_O and As_O, again consistent with the very large atomic size mismatch between Sb and O. It is therefore not expected that Sb will incorporate on the O site, instead substituting on the Sn site as a shallow donor.

C. Hydrogen-acceptor interactions

Since H is a shallow donor in SnO_2, strong Coulombic attraction with negatively ionized acceptors is expected, which can affect both their activation and solubility as previously reported for the group-IIIA impurities.[8] Among the group-V impurities, we have found that only N acts as an acceptor in SnO_2; we therefore restrict our discussion to N-H complexes in SnO_2. In the case of group-IIIA impurities it was found that the interstitial H bonds to a neighboring O atom.[8] In contrast, in the case of N substituting on the O site, interstitial H bonds directly to the impurity.

The binding energy between interstitial H and the N_O impurity is given by

$$E_b = E^f[N_O^-] + E^f[H_i^+] - E^f[(N_O\text{-}H_i)^0], \quad (6)$$

where $E^f[(N_O\text{-}H_i)^0]$ is the formation energy of the N-H complex. A positive value for E_b means that the neutral complex N_O-H_i is lower in energy than the isolated H_i^+ and N_O^- constituents. We find binding energies of 2.09 eV and 1.68 eV under O-rich and O-poor conditions, respectively. As mentioned in Sec. II B, NH_3 formation affects the N-H binding energy under O-poor conditions.

We note that the binding energy of the N-H complex is significantly larger than the binding energy for complexes between H and group-IIIA impurities.[8] This is due to the formation of a direct bond between H and nitrogen whereas in the case of group-IIIA impurities H_i^+ is bonded to a neighboring O atom. As shown in Fig. 7 and reflected in the reported binding energies, the neutral N-H complex is quite stable, with a lower formation energy than N_O and H_i separated, under both O-rich and O-poor conditions. This indicates that H can enhance the solubility of N in SnO_2.

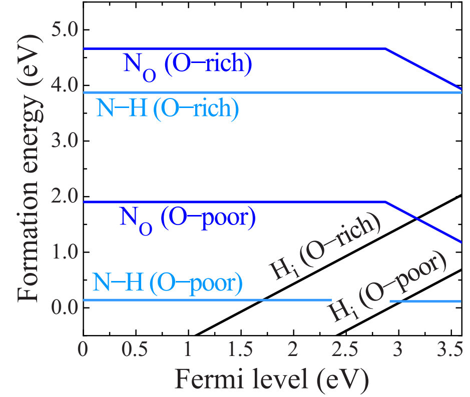

FIG. 7. (Color online) Calculated formation energies for substitutional N on the O site and its neutral complex with interstitial hydrogen. Bounds for the impurity and complex formation energies correspond to the extreme O-poor and O-rich limits.

We also calculated the stretch-mode vibrational frequency of the N-H bond in SnO_2 to provide a signature for experimental identification. We obtain a value of $\omega = 3266\ \text{cm}^{-1}$ by fitting the energy-displacement curve of the interstitial H, including anharmonic effects.[8] This frequency is slightly higher than the value for isolated interstitial hydrogen, which was determined to be $3245\ \text{cm}^{-1}$ by the same procedure.[8] The higher frequency of the N-H bond is indicative of a stronger bond exemplified by the large binding energy of this complex.

IV. CONCLUSION

We have performed a systematic study of the behavior of the group-V elements N, P, As and Sb as substitutional dopants in SnO_2. Using hybrid functional calculations, we have found that nitrogen prefers to incorporate on an oxygen site and acts as a very deep acceptor. P, As, and Sb strongly prefer to incorporate on Sn sites and act as shallow donors. These group-V elements are therefore clearly not suitable for p-type doping of SnO_2, while As and Sb appear as suitable n-type dopants with modest formation energies when substituting on the Sn site in more O-rich conditions. We also investigated the impact of codoping with hydrogen, which may enhance the solubility of N_O particularly under O-poor conditions. The resulting N-H complex shows a large binding energy, thus passivating the deep acceptor behavior of N_O.

ACKNOWLEDGMENTS

This work was supported by the NSF MRSEC Program under Award No. DMR05-20415 and by Saint-Gobain Research. It also made use of the CNSI Computing Facility under NSF under Grant No. CHE-0321368, as well as the TeraGrid resources supported by the NSF and provided by the TACC and SDSC under Grant No. DMR070072N. We are grateful to M. White, O. Bierwagen, and J. Speck for useful discussions.

[1] A. Kudo, H. Yanagi, K. Ueda, H. Hosono, and H. Kawazoe, Appl. Phys. Lett. **75**, 2851 (1999).
[2] R. G. Gordon, MRS Bull. **25**, 52 (2000).
[3] H. Hosono, Thin Solid Films **515**, 6000 (2007).
[4] I. Saadeddin, B. Pecquenard, J. P. Manaud, R. Decourt, C. Labrugère, T. Buffeteau, and G. Campet, Appl. Surf. Sci. **253**, 5240 (2007).
[5] Ç. Kılıç and A. Zunger, Appl. Phys. Lett. **81**, 73 (2002).
[6] J. Robertson and P. W. Peacock, Thin Solid Films **445**, 155 (2003).
[7] A. K. Singh, A. Janotti, M. Scheffler, and C. G. Van de Walle, Phys. Rev. Lett. **101**, 055502 (2008).
[8] J. B. Varley, A. Janotti, A. K. Singh, and C. G. Van de Walle, Phys. Rev. B **79**, 245206 (2009).
[9] S. Lany and A. Zunger, Phys. Rev. B **80**, 085202 (2009).
[10] A. Janotti and C. G. Van de Walle, Rep. Prog. Phys. **72**, 126501 (2009).
[11] J. Lyons, A. Janotti, and C. G. Van de Walle, Appl. Phys. Lett. **95**, 252105 (2009).
[12] J. M. Mochel, U.S. Patent No. 2,564,706 August 21, (1951).
[13] M. E. White, O. Bierwagen, M. Y. Tsai, and J. S. Speck, J. Appl. Phys. **106**, 093704 (2009).
[14] J. Heyd, G. E. Scuseria, and M. Ernzerhof, J. Chem. Phys. **118**, 8207 (2003); **124**, 219906 (2006).
[15] J. P. Perdew, K. Burke, and M. Ernzerhof, Phys. Rev. Lett. **77**, 3865 (1996).
[16] J. Paier, M. Marsman, K. Hummer, G. Kresse, I. C. Gerber, and G. G. Ángyán, J. Chem. Phys. **124**, 154709 (2006).
[17] M. Nagasawa and S. Shionoya, Phys. Lett. **22**, 409 (1966).
[18] F. Oba, A. Togo, I. Tanaka, J. Paier, and G. Kresse, Phys. Rev. B **77**, 245202 (2008).
[19] G. Kresse and J. Furthmüller, Phys. Rev. B **54**, 11169 (1996).
[20] G. Kresse and J. Furthmüller, Comput. Mater. Sci. **6**, 15 (1996).
[21] P. E. Blöchl, Phys. Rev. B **50**, 17953 (1994); G. Kresse and D. Joubert, *ibid.* **59**, 1758 (1999).
[22] H. J. Monkhorst and J. D. Pack, Phys. Rev. B **13**, 5188 (1976).
[23] C. Freysoldt, J. Neugebauer, and C. G. Van de Walle, Phys. Rev. Lett. **102**, 016402 (2009).
[24] K. Summitt, J. Appl. Phys. **39**, 3762 (1968).
[25] C. G. Van de Walle and J. Neugebauer, J. Appl. Phys. **95**, 3851 (2004).
[26] *CRC Handbook of Chemistry and Physics*, edited by D. R. Lide (CRC Press, Boca Raton, 2004), pp. 839–897, Sec. 5.
[27] A. A. Bolzan, C. Fong, B. J. Kennedy, and C. J. Howard, Acta Crystallogr., Sect. B: Struct. Sci. **53**, 373 (1997).
[28] R. M. Hazen and L. W. Finger, J. Phys. Chem. Solids **42**, 143 (1981).
[29] D. D. Wagman, W. H. Evans, V. B. Parker, R. H. Schumm, I. Halow, S. M. Bailey, K. L. Churney, and R. L. Nutall, J. Phys. Chem. Ref. Data **11**, 116 (1982).
[30] J.-M. Themlin, M. Chtaïb, L. Henrard, P. Lambin, J. Darville, and J.-M. Gilles, Phys. Rev. B **46**, 2460 (1992).
[31] T. Nagata, O. Bierwagen, M. E. White, M. Y. Tsai, and J. S. Speck, J. Appl. Phys. **107**, 033707 (2010).
[32] K. J. Button, C. G. Fonstad, and W. Dreybodt, Phys. Rev. B **4**, 4539 (1971).
[33] *Physics of Semiconductors: Proceedings of the 13th International Conference*, edited by F. G. Fumi (North-Holland, Amsterdam, 1976).
[34] N. Marom, O. Hod, G. E. Scuseria, and L. Kronik, J. Chem. Phys. **128**, 164107 (2008).
[35] W. A. Harrison, *Elementary Electronic Structure*, rev. ed. (World Scientific, Singapore, 2004).
[36] R. S. Katiyar, P. Dawson, M. H. Hargreave, and G. R. Wilkinson, J. Phys. C **4**, 2421 (1971).
[37] D. Stachel, I. Svoboda, and H. Fuess, Acta Crystallogr., Sect. C: Cryst. Struct. Commun. **51**, 1049 (1995).
[38] M. Jansen, M. Voss, and H. J. Deiseroth, Angew. Chem. **93**, 1023 (1981) (German edition).